Iterative Control of Piezoactuator for Evaluating Biomimetic, Cilia-Based Micromixing

Jiradech Kongthon and Santosh Devasia

***Abstract*—This work evaluates the use of different excitation waveforms to improve biomimetic-cilia-based mixing in microfluidic applications. A challenge in such studies is that, at high frequencies, vibrations in the piezoactuator can distort the achieved excitation waveform. An iterative approach is used in this work to account for the vibrational dynamics and avoid unwanted vibrations in the achieved excitation waveforms, and thereby enable the evaluation of different excitation waveforms on mixing. The main contribution of this work is to use these controlled, excitation waveforms for showing that (i) mixing time is substantially reduced by more than an order of magnitude with the use of cilia when compared to the case without cilia and (ii) mixing time with cilia can be further reduced, by more than half, by using an asymmetric excitation waveform when compared to symmetric sinusoidal excitation.**

***Index Terms*—Microsystems: nano- and micro-technologies; Mechatronic systems**

I. Introduction

BASED on biological cilia systems, e.g., [1]–[4], biomimetic, cilia-type, compliant actuators have been proposed for mixing and manipulation in liquid environments, e.g., see [5]–[11]. Recent works have shown that mechanical (sinusoidal) excitation of the cilia by using a piezoactuator to oscillate the cilia-chamber can improve mixing in microfludic devices [12], [13]. The current work aims to evaluate potential improvements in cilia-based mixing with different excitation waveforms of the cilia-chamber. A challenge in such evaluation studies is that, at high frequencies, vibrations in the piezoactuator can distort the achieved motion (excitation waveform) of the cilia-chamber, and thereby, limit the ability to evaluate the effect of a desired excitation waveform on mixing. An iterative feedforward approach [14] is used in this work to account for the vibrational dynamics of the piezoactuator, and reduce unwanted vibrations in the achieved excitation waveforms. The main contribution of this work is to use these controlled, excitation waveforms for showing that: (i) the average 90% mixing time is substantially reduced with the use of cilia when compared to the case without cilia by 13 times from 175s to 13.56s with sinusoidal excitation and (ii) the average 90% mixing time with cilia can be further reduced, about 2.6 times from 13.56s to 5.17s, by using an asymmetric excitation waveform when compared to symmetric sinusoidal excitation. Thus, the article shows that the choice of the excitation waveform can improve mixing performance with cilia, which suggests the need for further efforts in excitation-waveform optimization.

In general, micromixing can be improved by generating complex flows in the fluid to overcome the mixing-rate limits of laminar flows that are typical at the microscale. For example, passive techniques such as grooves can be used to generate chaotic folding and refolding of the liquid as it flows past the grooves to improve mixing, e.g., in [15]. Such flow-type mixing can be used when a sufficiently-large amount of sample is available to achieve the flow through the grooved channel. In contrast, if the amount of sample is limited, then batch-type mixing needs to be achieved in small chambers containing the sample. Batch mixing can be enhanced using a variety of actuation techniques such as high-frequency ultrasound excitation [16]–[18] and time-varying external magnetic fields [10], [19]–[21]. In the current work, cilia are excited by relatively-low-frequency oscillations of the chamber containing the sample when compared to higher-frequency ultrasound excitation. The low-frequency excitation used in this cilia-based method could reduce the damage of fragile samples that are susceptible to damage from high-frequency excitation [22]–[24]. However, further studies will be needed to evaluate the potential reduction in damage with the use of cilia-based micromixing.

II. Problem Formulation

A. System Description

The displacement transverse to the length (x) of a cilium was excited by using a piezoactuator (Burleigh PZS200) as shown in Figure 1a,b. The soft cilia were fabricated from polydimethylsiloxane (PDMS) using a silicon mold; detailed information on cilia fabrication and material properties can be found in [9]. The dimensions of the silicon mold used to fabricate the cilia were length ($L = 800\mu m$), height ($H = 45\mu m$), and width ($W = 10\mu m$) as in Figure 1c. The cilia and the fluid motion (Figure 1d) in the chamber were observed and evaluated using videos obtained with an optical microscope and an attached, digital, color CCD camera, as well as, still images (Pinnacle Studio Version 12). An example image of the resulting cilia vibration (due to the chamber oscillation) is shown in Figure 1e.

B. The Positioning Problem

An oscillatory excitation u_c of the cilia-chamber is achieved by using a piezo-based positioning system (referred to as the piezoactuator in the following) as shown in Figure 1. The motion of the base of each cilium is also u_c since the cilium base is attached to the chamber through a relatively-stiff PDMS structure. To evaluate the mixing achieved with different types of excitation waveforms (i.e., time profile of u_c), the

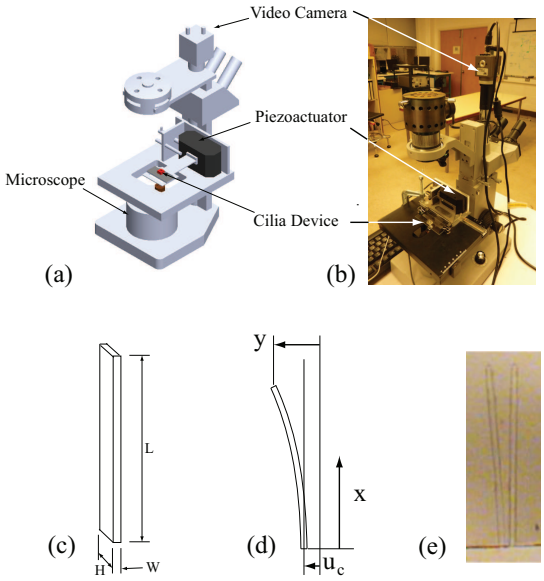

Fig. 1. Schematics of experiment for evaluating micromixing with cilia. Experimental setup: (a) schematic; and (b) photo. (c) Nominal cilium dimensions are length $L = 800\mu m$, width $W = 10\mu m$, and height $H = 45\mu m$. (d) Base motion $u_c(t)$ at $x = 0$ and tip motion $y(t)$ at the free end $x = L$ of a cilium. (e) Photo of a cilium in water excited by piezoactuator.

piezoactuator needs to position the chamber precisely along the desired waveform u_c. At high oscillation frequencies, vibrations in the piezoactuator positioning system can lead to distortions in the achieved position trajectory (excitation waveform), which make it challenging to evaluate specific excitation waveforms. The control goal is to correct for such vibration-caused distortions.

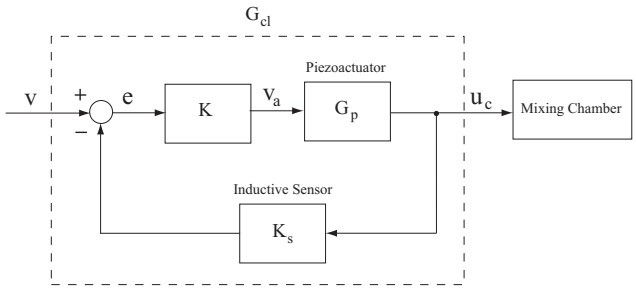

Fig. 2. Block diagram of the positioning system. The piezoactuator is represented by G_p, the achieved chamber motion u_c is measured with an inductive sensor with gain $K_s = 0.2$ (V/µm), and G_{cl} represents the closed-loop system.

III. Iterative Control of Piezoactuator

The model of the piezoactuator system, the design of the excitation frequency and waveforms, and iterative control to achieve the desired excitation waveform are discussed in this section.

A. Piezoactuator Model

A schematic of the positioning system is shown in Figure 2, where G_p represents the piezoactuator, the achieved chamber motion u_c is measured with an inductive sensor with gain $K_s = 0.2$ (V/µm), and G_{cl} represents the closed-loop system. The model of the closed-loop positioning system (G_{cl}) is obtained experimentally. Example experimental frequency responses of the closed loop system, obtained by using a dynamic signal analyzer (SRS Model SR785), are shown in Figure 3 for two cases: small amplitude; and large amplitude. For the small amplitude case, the input voltage V to the closed loop system was kept fixed at amplitude (0.1V) over different frequencies, which corresponds to a chamber-motion amplitude of 0.6µm (at low frequencies). For the large amplitude case, the displacement amplitude was fixed at a relatively-larger value of 5µm over different frequencies by varying the amplitude of the input voltage V. The substantial difference in the experimental frequency responses (in Figure 3) can be attributed to the significant hysteresis present in the system illustrated in Figure 4. This variation in the frequency response implies that linear models used to find feedforward inputs can have substantial error, which needs to be corrected.

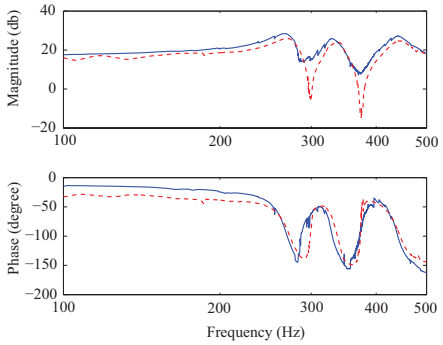

Fig. 3. Experimental frequency responses of the closed-loop system, G_{cl} in Figure 2 for two cases: small amplitude (dashed line); and large amplitude (solid line).

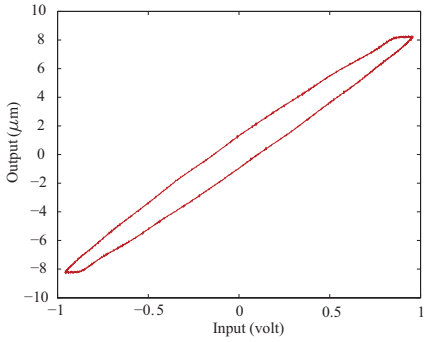

Fig. 4. Hysteresis in the closed-loop piezoactuator system obtained by applying sinusoidal input V to the closed-loop system at 20Hz and measuring the resulting output position u_c.

B. Choice of Control Method: Iterative Feedforward

Given a desired, excitation waveform $u_{c,d}$, the current article uses an iterative feedforward method to find the input V to achieve precision tracking of the desired waveform. It is noted that previous works have shown that iterative feedforward approaches can yield the highest tracking precision

in piezoactuator systems [25], [26]. In general, this approach can be applied with any feedback controller. In this work, the feedback was chosen as a simple proportional controller — its gain $K = 5$ was chosen to be as large as possible while maintaining sufficient gain and phase margins. However, the iterative approach used in this article can be used with more advanced feedback techniques as well.

C. Choice of Chamber Oscillation Frequency

The chamber oscillation frequency should be close to the cilia resonance frequency (in liquid) to achieve maximum excitation of the cilia [13]. To determine the chamber oscillation frequency (operating frequency) for mixing, the resonant frequencies of the cilia in liquid are found from the experimental frequency responses as shown in Figure 5 and Table I. As seen from Figure 5, the maximum amplitude of cilia response does not change significantly, if the operating frequency is varied from the mean value of 96.43Hz by one standard deviation.

In particular, with one standard deviation of the excitation frequency from the resonance, i.e., at 96.43Hz-1.27Hz and 96.43Hz+1.27Hz, the values of the response are $y/u_c = 3.50$ and $y/u_c = 3.487$ respectively, which represents no more than a 1.1% change from the maximum value of $y/u_c = 3.525$ at the resonance frequency 96.43Hz. Therefore, the associated change in the cilia response (because of potential variation in the resonance frequency from the mean value of 96.43Hz) is not expected to be substantial. Hence, in all experiments, the frequency ω_d of the periodic excitation trajectories was kept fixed at (approximately) the resonance frequency — $\omega_d = 96$Hz.

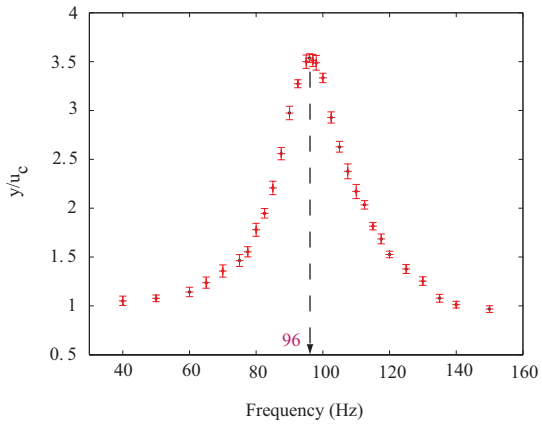

Fig. 5. Frequency response of seven runs of cilia. Dots represent the experimental data (mean values of seven runs of cilia), and bars represent the standard deviation $\pm\sigma$. Detailed models can be found in Refs. [13], [27].

D. Desired Excitation Waveforms

Two types of excitation waveforms are considered as shown in Figure 6: a symmetric sinusoidal excitation (used in previous studies [12], [13]); and a preliminary asymmetric (triangular) excitation. Tracking the preliminary triangular waveform $u_{c,p}$, with sharp changes in velocity at the turnarounds can be challenging because the corresponding velocity profile is discontinuous and the acceleration profile will be unbounded, which can require an infinite-bandwidth, unbounded input voltage V to perfectly track the waveform. Therefore, a filtered version of the preliminary triangular waveform $u_{c,p}$ is sought as the desired asymmetric waveform $u_{c,d}$ to meet actuator bandwidth and saturation limits.

Run Number	Resonant Frequency (Hz)
1	95
2	97
3	96
4	96
5	98
6	95
7	98
Mean	96.43
σ	1.27

TABLE I
RESONANT FREQUENCIES OF CILIA (SEVEN RUNS)

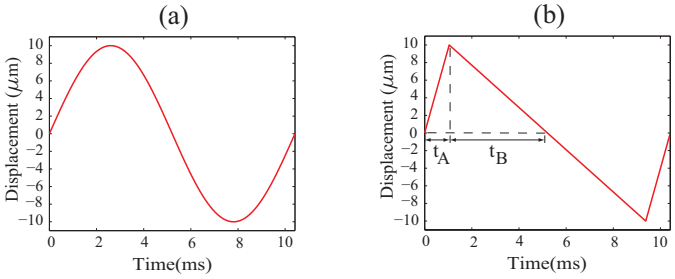

Fig. 6. Excitation waveforms u_c for one time period: (a) desired symmetric, sinusoidal waveform $u_{c,d}$, (b) preliminary asymmetric triangular waveform $u_{c,p}$, where the ratio $\alpha = t_A/t_B = 0.25$ is a measure of the asymmetry.

1) Optimal Inversion: A compromise between the goals of exactly tracking the preliminary triangular waveform $u_{c,p}$, and handling actuator bound and bandwidth limitations can be achieved using the optimal-inversion approach developed in [25].

The optimal inverse $V = V_{opt}$ is obtained by minimizing the following cost function

$$J(V) = \int_{-\infty}^{\infty} \{V^*(\omega)R(\omega)V(\omega) + E_P^*(\omega)Q(\omega)E_P(\omega)\}d\omega, \quad (1)$$

where $*$ denotes the complex conjugate transpose, the input V and output u_c are related through the system dynamics G_{cl}, and

$$E_P = u_{c,p} - u_c$$

is the positioning error with respect to the given preliminary excitation waveform $u_{c,p}$.

2) Choosing the Weights in the Cost Function: The terms $R(\omega)$ and $Q(\omega)$ (in Eq. 1) can be used to account for model uncertainty and piezoactuator-bandwidth limits by appropriately choosing the input-energy weight, $R(\omega)$ and the tracking-error E_P weight, $Q(\omega)$. In particular, the weights can be chosen such that good tracking is achieved in the low-frequency range (until 100Hz for the cilia-based mixing device) and to

reduce the emphasis on tracking at high frequencies where the model G_{cl} tends to become less accurate [28], e.g., beyond 500Hz for the current piezoactuator. This implies that the tracking-error weight Q should be larger than the input energy weight R in the low-frequency range and vice versa in the high-frequency range, as shown in Figure 7.

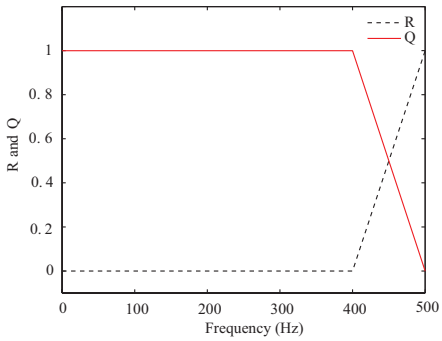

Fig. 7. Input energy weight, $R(\omega)$ and tracking-error weight, $Q(\omega)$ used in the cost function (in Eq. 1) to find the optimal inverse V_{opt} and the optimally filtered bandwidth-limited asymmetric waveform $u_{c,opt}$.

3) Optimal Inverse Feedforward: The optimal inverse input V_{opt} minimizing the cost function (in Eq. 1) can be found, for the single-input-single-output (SISO) case as [25]

$$\begin{aligned} V_{opt}(\omega) &= \left[\frac{{G_{cl}}^*(\omega)Q(\omega)}{R(\omega)+{G_{cl}}^*(\omega)Q(\omega)G_{cl}(\omega)}\right]u_{c,p}(\omega) \\ &= G_{cl,opt}^{-1}(\omega)u_{c,p}(\omega) \end{aligned} \tag{2}$$

and the time-domain signal for the feedforward input

$$V(t) = V_{opt}(t)$$

is then obtained through an inverse Fourier transform of $V_{opt}(\omega)$.

4) Optimal Asymmetric Waveform: The resulting optimal output $u_{c,opt}$ is given by

$$\begin{aligned} u_{c,opt}(\omega) &= G_{cl}(\omega)V_{opt}(\omega) \\ &= \left[\frac{{G_{cl}}^*(\omega)Q(\omega)G_{cl}(\omega)}{R(\omega)+{G_{cl}}^*(\omega)Q(\omega)G_{cl}(\omega)}\right]u_{c,p}(\omega) \\ &= \left[F_{opt}(\omega)\right]u_{c,p}(\omega) \end{aligned} \tag{3}$$

Therefore, the optimal waveform $u_{c,opt}$ can be considered as a filtered version (passing through filter $F_{opt}(\omega)$ determined by the frequency-dependent weights $R(\omega)$ and $Q(\omega)$) of the preliminary triangular waveform $u_{c,p}$ — the original and filtered waveforms are compared in Figure 8. The desired asymmetric waveform $u_{c,d}$ is then chosen to be the optimally-filtered waveform, i.e., $u_{c,d} = u_{c,opt}$, and the control objective is to track this optimally-filtered, desired, asymmetric waveform. Note from Eq. (3), that the chosen asymmetric waveform $u_{c,d}$ has finite bandwidth since the tracking weight is zero, $Q(\omega) = 0$, for higher frequencies $\omega \geq 500$Hz. Moreover, with the specific choice of the cost function — tracking error weight $Q(\omega)$ mostly one and the input weight $R(\omega)$ mostly zero (as in Figure 7) — the resulting optimal waveform is close to a truncated Fourier series of the preliminary triangular waveform, except for the harmonic between 400Hz and 500Hz.

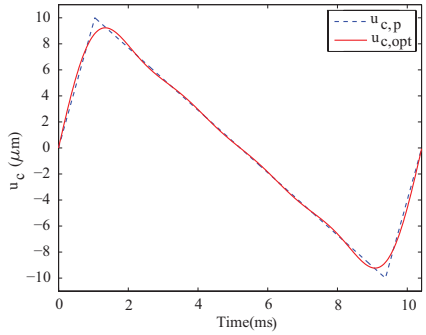

Fig. 8. Asymmetric waveform: (dashed line) original, infinite-bandwidth, triangular waveform; and (solid line) optimally-filtered, bandwidth-limited waveform.

E. Implementation: Iterative Inversion-Based Control

To account for modeling errors, the optimal inverse feedforward V_{opt} is computed (and corrected) iteratively as [29]

$$\begin{aligned} V_{opt,k}(\omega) = V_{opt,k-1}(\omega) \\ + \rho(\omega)G_{cl,opt}^{-1}(\omega)\left[u_{c,p}(\omega) - u_{c,k-1}(\omega)\right] \end{aligned} \tag{4}$$

for $k \geq 2$, where the initial input $V_{opt,1}(\omega)$ is

$$V_{opt,1}(\omega) = \left[G_{cl,opt}^{-1}(\omega)\right]u_{c,p}(\omega), \tag{5}$$

$\rho(\omega) \in \Re$ is the iteration gain, $u_{c,p}(\omega)$ is the Fourier transform of the preliminary trajectory, and $u_{c,k-1}(\omega)$ is the Fourier transform of the actual trajectory (experimentally) measured in the $(k-1)^{th}$ iteration step.

The iteration gain $\rho(\omega)$ should be chosen as large as possible to enable fast convergence; the maximum possible value can be estimated based on the anticipated modeling errors. The main criterion is to ensure that the iterative correction is in the right direction (phase criterion) — as shown in [29], the iteration gain $\rho(\omega)$ should satisfy

$$0 < \rho(\omega) < \frac{2cos(\triangle_\theta(\omega))}{\triangle_r(\omega)} = M(\omega) \tag{6}$$

where $\triangle_\theta(\omega)$ is the estimated phase error (difference in phase between the model and the actual system) and $\triangle_r(\omega)$ represents the estimated magnitude error (in terms of the ratio between the magnitudes of the model and the actual system) in the frequency response. These estimated errors are found using the two frequency responses (shown in Figure 3), and the estimated bound $M(\omega)$ on the iteration gain is shown in Figure 9, which has a minimum value of 0.8 in the computed frequency range. The actual bound (and the minimum) could be lower since the estimate is based on two measurements; moreover, noise can reduce the iteration gain as well as shown in [29]. Therefore, in the following, the iteration gain is chosen as a smaller value of 0.3 at all frequencies.

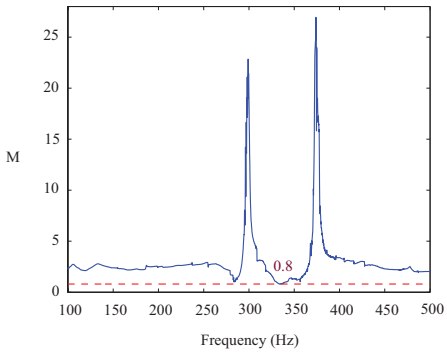

Fig. 9. The frequency dependent bound $M(\omega)$ (solid line) on the iteration gain $\rho(\omega)$ as in [29]. The minimum value (0.8) is shown as a dashed line.

F. Iterative Control Results

The results of the iterations are shown in Figure 10 and tabulated in Table II, which show that the iteration process substantially reduces the tracking error

$$E_k(t) = u_{c,opt}(t) - u_{c,k}(t). \tag{7}$$

In particular, the maximum tracking error

$$E_{k,max} = \max_{n\in[0,1,\ldots,N]} |E_k(t_n)|\,, \tag{8}$$

over all sampled time instants (t_n with $n \in [0,1,\ldots,N]$) in a time period $[0, 1/\omega_d]$, is reduced from an initial value of $2.71\mu\text{m}$ to a final value of $0.37\mu\text{m}$ in six iteration steps. Note that the final maximum error $E_{6,max}$ at the sixth iteration is small (1.85%) compared to the $20\mu\text{m}$ magnitude of the desired motion. Similarly, the root mean squared (rms) of the tracking error

$$E_{k,rms} = \sqrt{\frac{\sum_{i=1}^{N}[E_k(t_n)]^2}{N}} \tag{9}$$

is reduced from an initial value of $82.82\mu\text{m}$ to a final value of $8.51\mu\text{m}$ in six iteration steps. For clarity, the initial $u_{c,1}$ and final ($u_{c,6}$ at iteration step 6) waveforms are compared with the desired optimal waveform $u_{c,d} = u_{c,opt}$ in Figure 11.

Iteration Step k	$E_{k,max}$ μm	$E_{k,rms}$ μm
1	2.71	82.82
2	2.17	47.98
3	0.90	21.01
4	0.81	14.27
5	0.66	11.45
6	0.37	8.51

TABLE II
MAXIMUM $E_{k,max}$ AND RMS $E_{k,rms}$ TRACKING ERROR

IV. EXPERIMENTAL EVALUATION OF MIXING

The mixing of ink and water in an oscillating chamber is evaluated to show that (i) mixing time is substantially reduced with the use of cilia when compared to the case without cilia and (ii) mixing time with cilia can be further decreased by using an asymmetric excitation waveform when compared to a symmetric sinusoidal excitation.

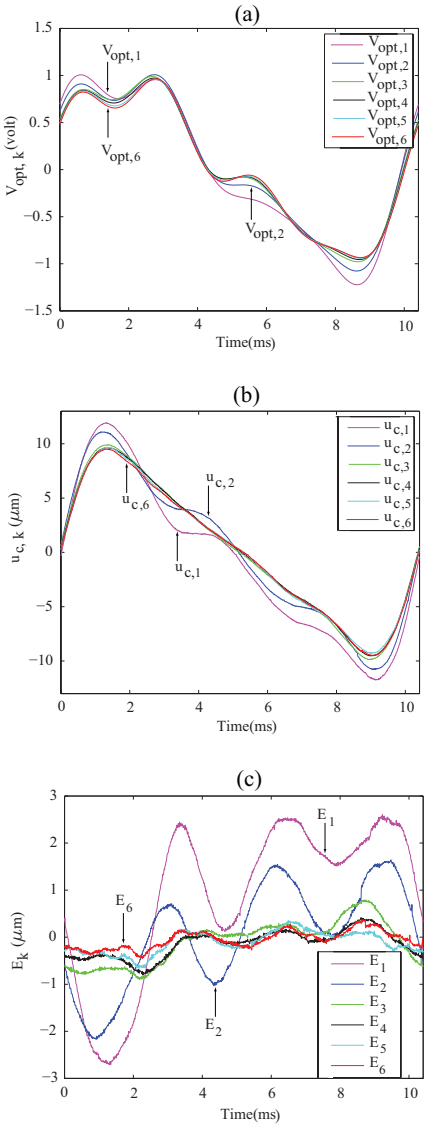

Fig. 10. Iteration results for iteration steps k from 1 to 6: (a) optimal inverse input $V_{opt,k}$; (b) experimentally measured waveform $u_{c,k}$; and (c) error in waveform $E_k(t) = u_{c,opt}(t) - u_{c,k}(t)$.

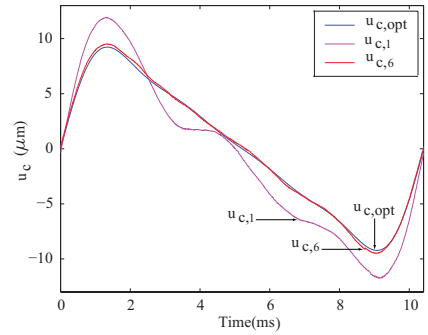

Fig. 11. Comparison of initial $u_{c,1}$ and final ($u_{c,6}$ at iteration step 6) waveforms with the desired, optimal, asymmetric waveform $u_{c,d} = u_{c,opt}$.

A. Procedure for Mixing Experiments

The procedure for the mixing experiment with cilia is described below. The procedure for the mixing experiments without cilia (i.e., vibration only) is the same as the case with cilia — except that cilia are not present in the chamber. For mixing experiments with cilia, three cilia were arranged in the mixing chamber as shown in Figure 12.

The cilia mixing device was attached to the piezoactuator as shown in Figure 1a,b. The cilia mixer system was positioned above an inverted microscope. After positioning the cilia mixer, de-ionized (DI) water (11μL) was added to the chamber using a pipette. Collapsed cilia, if any, were straightened by using tweezers. Next, 0.25μL of black ink (Drawing ink A, Pelikan, Hannover, Germany that is diluted 80 times with DI water) was released gently using a pipette at the center of the chamber under the water surface. The initial image of the ink drop (at time $t = 0s$) is shown in Figure 13. A thin PDMS sheet was placed above the chamber to enclose the mixing chamber to avoid evaporation of the solution during the mixing experiments. The PDMS cover did not suppress sloshing of the free surface because the solution volume together with the cilia-support structure created a maximum water height of 1.66mm, which did not reach the top of the chamber. Additionally, a support for the cover was added (as in Figure 12) to prevent the cover from sagging and touching the water surface.

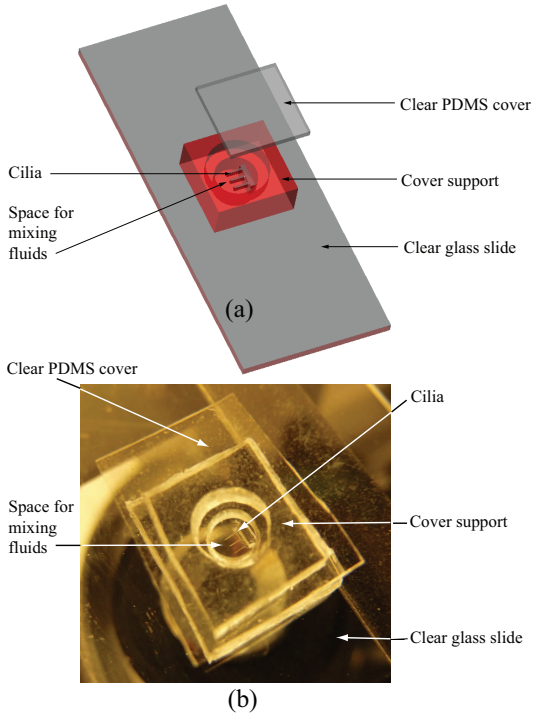

Fig. 12. (a) Schematic and (b) photo of setup of cilia device for mixing experiments in a 3mm diameter chamber.

Subsequently, the piezoactuator was used to oscillate the chamber perpendicular to the length of the cilia at an oscillation frequency of 96Hz. For the symmetric excitation case, the input V was chosen as a sinusoid, and for the asymmetric excitation case, the input V was chosen as the input $V_{opt,6}$ from the final (sixth) iteration step. In general, the mixing rate can be affected by the magnitude of the excitation. To enable comparisons between the different scenarios, the amplitudes of the waveforms were kept the same for all the experiments. Towards this, the amplitude of the input V to the closed-loop system (for each waveform) was scaled to ensure that the amplitude of the chamber oscillation u_c was kept the same (10μm) for both of the excitation waveforms.

Each mixing experiment (with and without cilia for the two different waveforms) was repeated seven times. During each mixing experiment, the initial image was captured after the addition of ink and after the thin PDMS sheet was used to cover the chamber but just before the start of the chamber oscillations with the piezoactuator. Preliminary experiments were performed to choose a sufficiently large time for the mixing experiments such that the mixing index (described in the section below) reaches a steady state value. Based on these preliminary studies, the time t_N for the final image was chosen as 50s for the case with cilia and 600s for the case without cilia. Additionally, the images were inspected to visually verify that they do not change significantly when the last images were collected.

The time for the mixing index to reach and stay within 90% of its final value is used to quantify and comparatively evaluate the mixing performance with and without cilia for the two different waveforms. A CCD camera, attached to the microscope as shown in Figure 1(a), was used to video-record the mixing process for evaluation — samples of the acquired images are shown in Figure 13. When the fluid sloshing is excited (after the ink is dropped), sometimes effects of the light sources and shadows are seen in the images, e.g., the bright spots seen in Figure 13(d). These bright spots do not appear before the motion is initiated and after the motion is stopped, as shown in Figure 14. Such visual inspections were done after the motion was turned off to ensure that these features do not remain, e.g., due to stable islands of unmixed regions. Moreover, these features in the image do not change at steady state and are, therefore, accounted-for by comparing, for different experiments, the time for the mixing index to reach and stay within 90% of its steady-state value.

B. Quantifying Mixing

The mixing was quantified by comparing images from the video recording of the mixing process using a mixing index I_{mix} developed in [12], which is a discrete version of the continuous time mixing index defined in [30]. The mixing index, which is a measure of relative mixing, is initially 0 and approaches 1 when the fluids become fully mixed, is given by

$$I_{mix}(t_k) = \frac{1}{I_{ss}}\left[1 - \frac{\sum_{p=1}^{P} |C_p(t_k) - C_p(t_N)|}{\sum_{p=1}^{P} |C_p(t_0) - C_p(t_N)|}\right] \qquad (10)$$

where $[t_k]_{k=1}^{N}$ represents the different time instants when the images are evaluated, N is the total number of images, P is the number of pixels in each of the images, $C_p(t_k)$ is the color

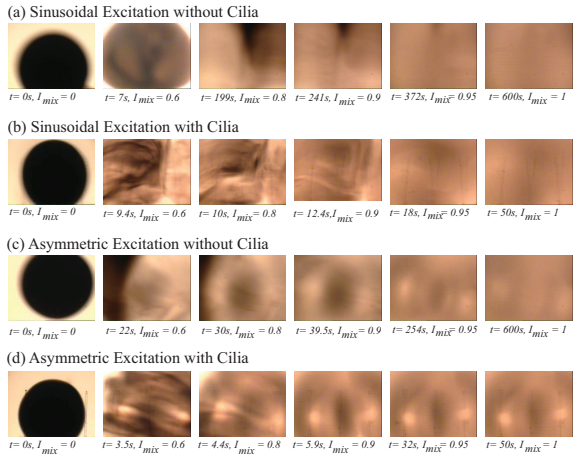

Fig. 13. Sample images of the mixing process at different time instants t for Run 1: (a) sinusoidal excitation without cilia (b) sinusoidal excitation with cilia; (c) asymmetric excitation without cilia; and (d) asymmetric excitation with cilia.

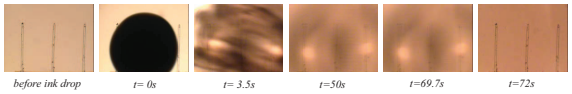

Fig. 14. Sample images of the mixing process at different time instants t for Run 1 of asymmetric excitation with cilia (as in Figure 13d), showing images before, during, and after excitation. The input V to the piezoactuator was stopped at 69.7s and the chamber stopped moving by 72s.

of p^{th} pixel at time instant t_k, and the normalization factor I_{ss} is given by

$$I_{ss} \;=\; \left| 1 - \frac{\sum_{p=1}^{P} |C_p(t_{N-1}) - C_p(t_N)|}{\sum_{p=1}^{P} |C_p(t_0) - C_p(t_N)|} \right|. \qquad (11)$$

Each image used in this analysis is composed of an array of 720 pixels by 480 pixels, and the color of each pixel C is a vector of three values

$$C \;=\; [R \;\; G \;\; B]$$

that represents red, green, and blue (RGB) color with values between 0 and 255. Given any two pixel colors C_i and C_j, the difference between them (used in Eqs. 10, 11) is defined as

$$|C_i - C_j| \;=\; |R_i - R_j| + |G_i - G_j| + |B_i - B_j|.$$

As the mixing progresses and reaches a steady state (i.e., as t_k approaches t_N), the difference between the color of the corresponding pixels in the images becomes small, which tends to increase the values of I_{mix} from an initial value of zero towards one. The normalization factor I_{ss} in Eq. (11) uses the last two images to make the mixing index close to one when the mixing process reaches steady state and the images become similar. This is necessary because noise in the image (partly due to the oscillation) prevents the final value from reaching one without the normalization, i.e., when the normalization factor is chosen as $I_{ss} = 1$ in Eq. (10). To evaluate the mixing performance and determine the effect of the input waveform, two different excitation waveforms (symmetric and asymmetric) are used to oscillate the mixing chamber for each case: with and without cilia.

C. Mixing Results

The mixing time is substantially reduced with cilia when compared to the case without cilia and it is further decreased by using asymmetric excitation compared to the case with symmetric sinusoidal excitation. The reduction in mixing time with the cilia is visually observable in the images shown in Figure 13 for Run 1. For example, to reach the 90% mixing time for Run 1 (corresponding to the images on the 4th column), the mixing takes 12.4s with the cilia whereas it takes 241s for the case without the cilia for the sinusoidal excitation. The mixing time is further decreased by using asymmetric excitation compared to the case with symmetric sinusoidal excitation. For example, in Figure 13 with the use of the symmetric sinusoidal excitation, the mixing for Run 1 takes 12.4s with the cilia whereas with the use of the asymmetric excitation it takes 5.9s for the case with the cilia to reach the 90% mixing time.

The trends in the reduction in mixing time is also seen in averaged values over several experiments. The time variation of the mixing index (without and with cilia) are shown in Figures 15 and 16 and the 90% mixing time for the different experiments are presented in Tables III and IV. In particular, (i) the mixing time 90% is substantially reduced with the use of cilia when compared to the case without cilia by 13 times from $175s$ to $13.56s$ (with sinusoidal excitation) and (ii) the 90% mixing time with cilia is further reduced (about 2.6 times from $13.56s$ to $5.17s$) by using the asymmetric excitation waveform when compared to the symmetric sinusoidal excitation. Thus, the experimental results show that the mixing time is substantially reduced with cilia when compared to the case without cilia. Moreover, the mixing time is further decreased by applying the asymmetric excitation waveform to oscillate the mixing chamber when compared to the case of the symmetric sinusoidal excitation in previous studies [12], [13].

Run Number	Mixing Time without Cilia (s)	Mixing Time with Cilia (s)
1	241.0	12.4
2	182.5	12.2
3	122.0	13.0
4	155.5	14.8
5	230.0	17.3
6	157.0	13.5
7	137.0	11.7
Mean	175.0	13.56
σ	45.45	1.94

TABLE III
MIXING TIME(s) FOR SINUSOIDAL EXCITATION, QUANTIFIED BY THE TIME FOR THE MIXING INDEX I_{mix} IN EQ. (10) TO REACH AND STAY WITHIN 90% OF ITS FINAL VALUE, WITHOUT AND WITH CILIA

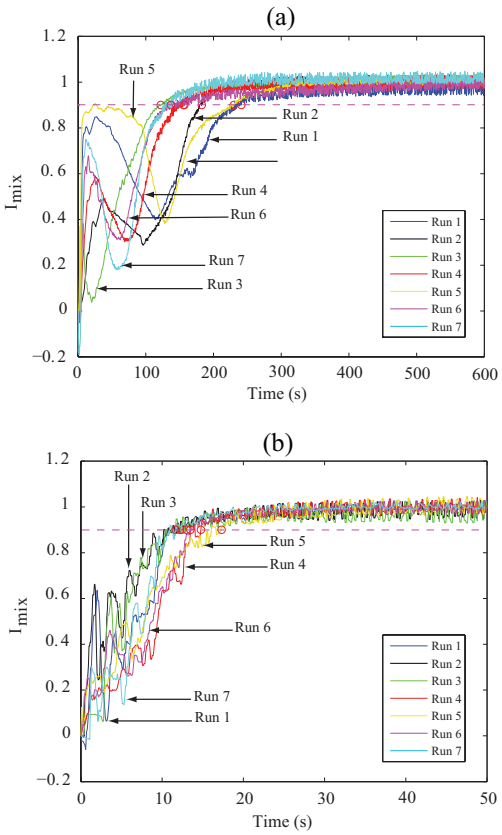

Fig. 15. Mixing indices for devices with : (a) sinusoidal excitation without cilia, (b) sinusoidal excitation with cilia.

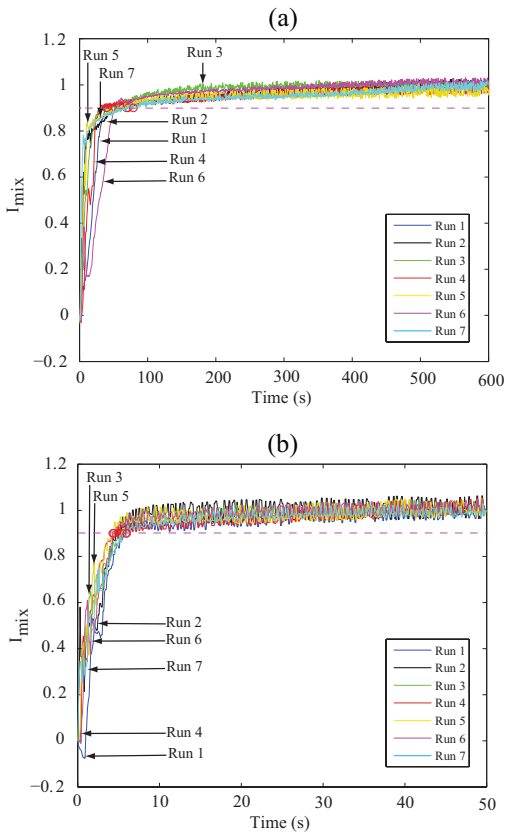

Fig. 16. Mixing indices for devices with : (a) asymmetric excitation without cilia, (b) asymmetric excitation with cilia.

Run Number	Mixing Time without Cilia (s)	Mixing Time with Cilia (s)
1	39.5	5.9
2	69.0	5.0
3	48.0	5.4
4	41.0	5.2
5	71.0	4.4
6	52.5	4.3
7	79.0	6.0
Mean	57.14	5.17
σ	15.74	0.67

TABLE IV
MIXING TIME(s) FOR ASYMMETRIC EXCITATION, QUANTIFIED BY THE TIME FOR THE MIXING INDEX I_{mix} IN EQ. (10) TO REACH AND STAY WITHIN 90% OF ITS FINAL VALUE, WITHOUT AND WITH CILIA

D. Discussion of Results

Although the asymmetric excitation leads to faster mixing, it cannot be caused by a substantial change in the cilia motion between the symmetric and asymmetric excitation waveforms. This is because the cilia dynamics is only substantial near the first resonance (at around 96Hz) and therefore, the higher harmonics in the excitation waveform does not lead to substantial cilia vibration — the cilia motion is expected to remain sinusoidal due to the response caused by the main harmonic in the excitation waveform at 96Hz. Nevertheless, the asymmetric excitation can lead to increased velocities of particles in the fluid when compared to the symmetric excitation due to increased net forcing in each oscillation period. This can lead to faster mixing. To evaluate this, the motion of particles in the flow was evaluated using polymer microspheres (crosslinked poly(styrene/divinylbenzene), mean diameter of 18.97μm, PS07N/1733, Bangs Laboratories, Inc.) with the same operating conditions as the ink-mixing experiment (without the ink) for all four cases: (a) sinusoidal excitation without cilia; (b) sinusoidal excitation with cilia, (c) asymmetric excitation without cilia, and (d) asymmetric excitation with cilia. The results show that the microspheres actuated by the asymmetric excitation waveform have greater average speed compared to the ones with the symmetric excitation waveform as shown in Table V for both cases — with and without cilia. This is to be expected since asymmetric excitation leads to a nonzero impulse over each time period when compared to symmetric excitation. Similarly, cilia also lead to increased speed of the particles, for both cases, symmetric and asymmetric excitation. Thus, there appears to be two effects: (i) the use of asymmetric excitation waveform increases the speed of particles — the increased particle speed can lead to faster mixing, with mixing time reduced by more than half; and (ii) the use of cilia increases the rate of mixing further for, both, symmetric and asymmetric excitation cases — the mixing time is reduced further by about more than an order of magnitude in each case.

In summary, the results show that the choice of the excitation waveform can improve the mixing performance, further, for cilia-based devices. This suggests the need for additional

Excitation Waveform	Speed without Cilia ($\mu m/s$)	Speed with Cilia ($\mu m/s$)
Sinusoidal	335.67±47.01	1026.35±214.46
Asymmetric	616.13±151.06	2317.16±304.22

TABLE V
SPEED, MEAN VALUE AND STANDARD DEVIATION FOR 10 MICROSPHERES FOR EACH OF THE FOUR CASES — WITHOUT AND WITH CILIA, AND SYMMETRIC-SINUSOIDAL AND ASYMMETRIC EXCITATION

research in excitation-waveform optimization — this is part of our ongoing efforts.

V. CONCLUSIONS

An iterative, optimal-inversion-based control was used to achieve precision control of excitation waveforms applied to a novel biomimetic cilia-based mixer. Experimental results were presented to show that (i) the mixing time was substantially reduced with the use of cilia when compared to the case without cilia by 13 times (with sinusoidal excitation) and (ii) the mixing time with cilia can be further reduced (about 2.6 times) by using an asymmetric excitation waveform when compared to the previous use of symmetric sinusoidal excitation. The results illustrate the need for additional optimization studies of the excitation waveform to further improve the mixing rate in cilia-based devices.

ACKNOWLEDGMENT

The authors would like to thank the National Science Foundation for the support through Grants CMII 0624597 and 1000404, and Dr. Kieseok Oh and Brandon Smith for their help with the cilia fabrication and the development of the mixing index used in this research.

REFERENCES

[1] C. Brennen, "An oscillating-boundary-layer theory for ciliary propulsion," *Journal of Fluid Mechanics*, vol. 65, no. 4, pp. 799–824, 1974.
[2] E. O. Tuck, "A note on a swimming problem," *Journal of Fluid Mechanics*, vol. 31, pp. 305–308, 1968.
[3] M. Ramia, D. L. Tullock, and N. Phanthien, "The role of hydrodynamic interaction in the locomotion of microorganisms," *Biophysical Journal*, vol. 65, pp. 755–778, 1993.
[4] S. Gueron and K. Levit-Gurevich, "Computation of the internal forces in cilia: Application to ciliary motion, the effects of viscosity, and cilia interactions," *Biophysical Journal*, vol. 74, pp. 1658–1676, 1998.
[5] Z. Chen, S. Shatara, and X. Tan, "Modeling of biomimetic robotic fish propelled by an ionic polymer-metal composite caudal fin," *IEEE-ASME Transactions on Mechatronics*, vol. 15, no. 3, pp. 448–459, June 2010.
[6] B. Behkam and M. Sitti, "Design methodology for biomimetic propulsion of miniature swimming robots," *ASME Journal of Dynamic Systems Measurement and Control*, vol. 128, no. 1, pp. 36–43, March 2006.
[7] P. Alvarado and K. Youcef-Toumi, "Design of machines with compliant bodies for biomimetic locomotion in liquid environments," *ASME Journal of Dynamic Systems Measurement and Control*, vol. 128, no. 1, pp. 3–13, March 2006.
[8] M. T. A. Saif, B. E. Alaca, and H. Sehitoglu, "Analytical modeling of electrostatic membrane actuator for micro pumps," *IEEE Journal of Microelectromechanical Systems*, vol. 8, no. 3, pp. 335–345, September 1999.
[9] K. Oh, J. Chung, S. Devasia, and J. J. Riley, "Bio-mimetic silicone cilia for microfluidic manipulation," *Lab on a Chip by the Royal Society of Chemistry*, vol. 9, no. 11, pp. 1561–1566, 2009.
[10] V. V. Khatavkar, P. D. Anderson, J. M. J. den Toonder, and H. E. H. Meijer, "Active micromixer based on artificial cilia," *Physics of Fluids*, vol. 19, no. 8, p. # 083605, August 2007.
[11] R. Dreyfus, J. Baudry, M. Roper, M. Fermigier, H. Stone, and J. Bibette, "Microscopic artificial swimmers," *Nature*, vol. 437, no. 7060, pp. 862–865, October 6 2005.
[12] K. Oh, B. Smith, S. Devasia, J. Riley, and J.-H. Chung, "Characterization of mixing performance for bio-mimetic silicone cilia," *Microfluid. Nanofluid.*, vol. 9, no. 4-5, pp. 645–655, October 2010.
[13] J. Kongthon, J. Chung, J. J. Riley, and S. Devasia, "Dynamics of cilia-based microfluidic devices," *ASME Journal of Dynamic Systems, Measurement and Control*, vol. 133, pp. 051 012–1–051 012–11, September 2011.
[14] S. Devasia, E. Eleftheriou, and S. O. R. Moheimani, "A survey of control issues in nanopositioning," *IEEE Transactions on Control Systems Technology*, vol. 15(5), pp. 802–823, Sept, 2007.
[15] A. Stroock, S. Dertinger, A. Ajdari, I. Mezic, H. Stone, and G. Whitesides, "Chaotic mixer for microchannels," *Science*, vol. 295, no. 5555, pp. 647–651, January 25 2002.
[16] H. Monnier, A. M. Wilhelm, and H. Delmas, "Effects of ultrasound on micromixing in flow cell," *Chemical Engineering Science*, vol. 55, pp. 4009–4020, 2000.
[17] G. G. Yaralioglu, I. O. Wygant, T. C. Marentis, and B. T. Khuri-Yakub, "Ultrasonic mixing in microfluidic channels using integrated transducers," *Analytical Chemistry*, vol. 76, pp. 3694–3698, 2004.
[18] J. Hawkes, R. Barber, D. Emerson, and W. Coakley, "Continuous cell washing and mixing driven by an ultrasound standing wave within a microfluidic channel," *Lab on a Chip*, vol. 4, no. 5, pp. 446–452, 2004.
[19] M. Grumann, A. Geipe, L. Riegger, R. Zengerle, and J. Ducree, "Batch-mode mixing on centrifugal microfluidic platforms," *Lab on a Chip*, vol. 5, no. 5, pp. 560–565, 2005.
[20] M. Herrmann, T. Veres, and M. Tabrizian, "Enzymatically-generated fluorescent detection in micro-channels with internal magnetic mixing for the development of parallel microfluidic elisa," *Lab on a Chip*, vol. 6, no. 4, pp. 555–560, 2006.
[21] M. Vilfan, A. Potocvnik, B. Kavcvicv, N. Osterman, I. Poberaj, A. Vilfan, and D. Babic, "Self-assembled artificial cilia," *Proceedings of the National Academy of Sciences of the USA*, vol. 107, no. 5, pp. 1844–1847, February 2 2010.
[22] D. L. Miller, R. M. Thomas, and R. L. Buschbom, "Comet assay reveals DNA strand breaks induced by ultrasonic cavitation in vitro," *Ultrasound in Med. and Biol.*, vol. 21, no. 6, pp. 841–848, 1995.
[23] E. A. Mansur, Y. Mingxing, W. Yundong, and D. Youyuan, "A state-of-the-art review of mixing in microfluidic mixers," *Chinese Journal of Chemical Engineering*, vol. 16, no. 4, pp. 503–516, August 2008.
[24] M. M. Rageh, A. El-Lakkani, M. H.M.Ali, A. M. M. A. El-Fattah, and A. E.-G. Raafat, "Effect of high power ultrasound on aqueous solution of DNA," *International Journal of Physical Sciences*, vol. 4, no. 2, pp. 063–068, February 2009.
[25] J. Dewey, K. Leang, and S. Devasia, "Experimental and theoretical results in output- trajectory redesign for flexible structures," *ASME Journal of Dynamic Systems, Measurement, and Control*, vol. 120(4), pp. 456–461, December, 1998.
[26] G. M. Clayton, S. Tien, K. K. Leang, Q. Zou, and S. Devasia, "A review of feedforward control approaches in nanopositioning for high speed spm," *ASME Journal of Dynamic Systems, Measurement and Control*, vol. 131(6), pp. 1–19, Article 061 001, November, 2009.
[27] J. Kongthon, B. Mckay, D. Iamratanakul, K. Oh, J. Chung, J. J. Riley, and S. Devasia, "Added-mass effect in modeling of cilia-based devices for microfluidic systems," *ASME Journal of Vibration and Acoustics*, vol. 132, pp. 024 501–1–024 501–7, April 2010.
[28] S. Devasia, "Should model-based inverse inputs be used as feedforward under plant uncertainty?" *IEEE Transactions on Automatic Control*, vol. 47(11), pp. 1865–1871, 2002.
[29] S.Tien, Q. Zou, and S. Devasia, "Iterative control of dynamics-coupling-caused errors in piezoscanners during high-speed AFM operation," *IEEE Transactions on Control Systems Technology*, vol. 13, no. 6, pp. 921–931, November, 2005.
[30] N. L. Jeon, S. K. W. Dertinger, D. T. Chiu, I. S. Choi, A. D. Stroock, and G. M. Whitesides, "Generation of solution and surface gradients using microfluidic systems," *Langmuir*, vol. 16, pp. 8311–8316, July 2000.